JOURNAL OF AIRCRAFT
Vol. 38, No. 5, September–October 2001

Fluid-Structure Interactions of a Round Parachute: Modeling and Simulation Techniques

Keith R. Stein* and Richard J. Benney†
U.S. Army Soldier and Biological Chemical Command, Natick, Massachusetts 01760
Tayfun E. Tezduyar‡
Rice University, Houston, Texas 77005
and
John W. Leonard§ and Michael L. Accorsi¶
University of Connecticut, Storrs, Connecticut 06269

A parallel computational technique is presented for carrying out three-dimensional simulations of parachute fluid-structure interactions, and this technique is applied to simulations of airdrop performance and control phenomena in terminal descent. The technique uses a stabilized space-time formulation of the time-dependent, three-dimensional Navier–Stokes equations of incompressible flows for the fluid dynamics part. Turbulent features of the flow are accounted for by using a zero-equation turbulence model. A finite element formulation derived from the principle of virtual work is used for the parachute structural dynamics. The parachute is represented as a cable-membrane tension structure. Coupling of the fluid dynamics with the structural dynamics is implemented over the fluid-structure interface, which is the parachute canopy surface. Large deformations of the structure require that the fluid dynamics mesh is updated at every time step, and this is accomplished with an automatic mesh-moving method. The parachute used in the application presented here is a standard U.S. Army personnel parachute.

Introduction

FLUID-STRUCTURE interactions (FSI) are involved at all stages of airdrop systems performance, including initial deployment, during inflation, terminal descent (or gliding/maneuvering for steerable parachutes), and soft landing (i.e., retraction for round parachutes, flared landing for ram-air parachutes). The interaction between the parachute system and the airflow around it is dominant in most parachute operations, and thus the ability to simulate parachute FSI is recognized within the parachute research community as a serious challenge.[1–6] In this paper a description is given of current efforts to develop a general-purpose computer model that can accurately predict three-dimensional FSI for various parachute systems under different performance stages. Here, the focus is on the FSI performance during the terminal descent stage to include riser control performance. Issues involved in performing simulations with the current model will be presented, including the finite element formulations, coupling methods, mesh moving methods, and implementation on parallel supercomputers.

The parallel computational technique presented here targets three-dimensional simulations of parachute FSI, with application to airdrop performance and control phenomena in terminal descent. The technique is based on the deforming-spatial-domain/stabilized space-time (DSD/SST) formulation[7,8] of the time-dependent, three-dimensional Navier–Stokes equations of incompressible flows for the fluid dynamics (FD) part. Turbulent features of the flow are accounted for by using a Smagorinsky turbulence model.[9] A finite element formulation derived from the principle of virtual work is used for the structural dynamics (SD).[10,11] The coupling between the FD and the SD is enforced over the fluid-structure interface, which is the canopy surface. Large deformations of the structure are handled by updating the FD mesh with an automatic mesh-moving scheme and remeshing as needed. The DSD/SST procedure is well suited for problems involving spatial domains changing with time, such as those encountered during parachute FSI.[12] This formulation has been well tested and applied to a large variety of fluid dynamics problems involving moving boundaries and interfaces. In the space-time formulation the finite element interpolation functions vary both spatially and temporally, and this automatically takes into account changes in the spatial domain.

In recent years the DSD/SST procedure has been applied to a variety of FSI problems. Preliminary DSD/SST simulations were successfully performed to simulate FSI behaviors for flow problems involving moving cylinders and aerofoils.[13,14] Later, the approach was applied to simulate the FSI response of a flexible pipe to internal flow[15] and to two-phase FSI flow problems including interior ballistics.[16] Recently, the approach has been used to predict the FSI response for the inflation of an axisymmetric cable-membrane parachute structure,[17] to predict the steady-state descent characteristics for a ram-air parachute system,[4] and to predict steady-state characteristics for a fully inflated T-10 parachute system under controlled conditions (i.e., pinned at the payload and subjected to a uniform freestream flowfield).[3] Finally, a series of FSI simulations[18] and concurrent wind-tunnel experiments[19] have been performed for a set of cross-parachute models as a first step toward validation of this parachute FSI simulation capability.

For the FSI problems presented, special attention is given to the transfer of coupling information between "compatible" and "incompatible" FD and SD interface meshes (i.e., parachute canopy surface meshes). For compatible meshes the FD and SD have nodally equivalent interface meshes, and the transfer of coupling information is straightforward. For incompatible meshes coupling information must be transferred through more complicated projection strategies.[4,20]

Received 20 February 2000; revision received 25 October 2000; accepted for publication 10 November 2000.

*Aerospace Engineer, Soldier Systems Center.
†Aerospace Engineer, Soldier Systems Center. Senior Member AIAA.
‡James F. Barbour Professor in Engineering and Chairman, Mechanical Engineering and Materials Science.
§Professor, Department of Civil and Environmental Engineering.
¶Professor, Department of Civil and Environmental Engineering. Member AIAA.

Governing Equations

Fluid Dynamics

Let $\Omega_t \subset \mathbb{R}^{n_{sd}}$ and $(0, T)$ be the spatial and temporal domains, respectively, where n_{sd} is the number of space dimensions, and let Γ_t denote the boundary of Ω_t. The subscript t implies the time dependence of the spatial domain. The spatial and temporal coordinates are denoted by $\boldsymbol{x} = (x, y, z)$ and $t \in (0, T)$. The Navier–Stokes equations of incompressible flows are

$$\rho\left(\frac{\partial \boldsymbol{u}}{\partial t} + \boldsymbol{u}\cdot\nabla\boldsymbol{u} + \boldsymbol{f}\right) - \nabla\cdot\boldsymbol{\sigma} = 0 \qquad \text{on} \qquad \Omega_t \forall t \in (0, T) \tag{1}$$

$$\nabla\cdot\boldsymbol{u} = 0 \qquad \text{on} \qquad \Omega_t \forall t \in (0, T) \tag{2}$$

Here ρ, $\boldsymbol{u}$, $\boldsymbol{f}$, and $\boldsymbol{\sigma}$ are the density, velocity, external body force, and stress tensor, respectively. For the problems under consideration, the fluid is assumed Newtonian, and the dynamic viscosity is modified locally using a Smagorinsky turbulence model.[9] Dirichlet and Neumann-type boundary conditions are prescribed on $(\Gamma_t)_g$ and $(\Gamma_t)_h$, respectively, where $(\Gamma_t)_g$ and $(\Gamma_t)_h$ are complementary subsets of the boundary Γ_t. The initial condition on the velocity is divergence free.

Structural Dynamics

Let $\Omega_t^s \subset \mathbb{R}^{n_{xd}}$ be the spatial domain bounded by Γ_t^s, where $n_{xd} = 2$ for membranes and $n_{xd} = 1$ for cables. The boundary Γ_t^s is composed of $(\Gamma_t^s)_g$ and $(\Gamma_t^s)_h$. Here, the superscript s corresponds to the cable-membrane structure. The equations of motion for the structural system are

$$\rho^s\left(\frac{\mathrm{d}^2\boldsymbol{y}}{\mathrm{d}t^2} - \boldsymbol{f}^s\right) - \nabla\cdot\boldsymbol{\sigma}^s = 0 \qquad \text{on} \qquad \Omega_t^s \tag{3}$$

where $\boldsymbol{y}$, ρ^s, $\boldsymbol{f}^s$, and $\boldsymbol{\sigma}^s$ are the displacement, material density, external body forces, and Cauchy stress tensor, respectively. For the problems under consideration, we assume large displacements and rotations but small strains. Thus, constitutive relationships are based on Hookean materials with linear-elastic properties.

Finite Element Formulations

Fluid Dynamics

To handle the time-variant spatial domains encountered in parachute problems, we employ the DSD/SST finite element formulation.[7,8] In this formulation the finite element interpolation polynomials are functions of both space and time, and the stabilized variational formulation of the problem is written over the associated space-time domain. This stabilized formulation automatically takes into account deformations in the spatial domain and protects the computation against numerical oscillations. This method has been applied to a large number of problems with moving boundaries and interfaces. The DSD/SST method used in this paper is based on the streamline-upwind/Petrov–Galerkin (SUPG)[21] and pressure-stabilizing/Petrov–Galerkin (PSPG)[22] stabilization techniques. The SUPG method is one of the most widely used stabilization methods. The PSPG formulation assures numerical stability while allowing the use of equal-order interpolation functions for velocity and pressure. These stabilization techniques also prevent numerical oscillations and instabilities for flows involving high Reynolds numbers and boundary layers, without introducing excessive numerical dissipation.

Structural Dynamics

A semidiscrete finite element formulation for the SD equations of motion is obtained from the principle of virtual work. Finite displacements of the structure are taken into account by using a total Lagrangian description of the problem. In addition to membrane and cable elements, a variety of parachute-specific features have been incorporated into the SD solver to include truss and concentrated-mass elements (representing the payload), drag force approximations for cables and concentrated masses, and time-variant cable lengths (for control line pulls, reefing, etc.). The interested reader is directed to Benney et al.[11,23] for further details.

Mesh-Moving Strategy

To handle changes in the spatial domain caused by parachute canopy deformations, a suitable mesh-moving scheme is necessary. Efficient special purpose mesh-moving algorithms can be designed for problems where parachute motion is somewhat predictable. For example, Kalro and Tezduyar[4] utilized an algebraic scheme to handle the FSI-induced motions of a ram-air parachute system. A more general purpose mesh-moving scheme is needed for problems with arbitrary and complex deformations. We use an automatic mesh-moving scheme for the problems addressed. In this scheme the fluid mesh is treated as a linearly elastic pseudosolid that deforms as dictated by the motion of the surface boundaries of the fluid domain.[24] This scheme introduces an additional computational cost associated with the mesh-moving equations, but is well suited for handling the complex geometries and arbitrary motions for this class of problems. The solution for the pseudosolid has no physical significance in itself. Its sole purpose is to deform the FD mesh to handle, with minimal mesh distortion, motions and deformations in mesh boundaries and interfaces.

Fluid-Structure Coupling

The fluid-structure coupling occurs at the FSI interface, which is in this case the parachute canopy surface. We use an iterative coupling approach, with individual systems of equations being solved for the fluid and the structure. Coupling is achieved through the transfer of FSI information between the fluid and structure within a nonlinear iteration loop, with multiple nonlinear iterations improving the convergence of the coupled system. Displacements from the SD solution are treated as Dirichlet boundary conditions in the mesh-moving scheme. Displacement rates from the SD solution are treated as Dirichlet boundary conditions in the FD solver. In return, parachute surface tractions from the fluid are used as distributed forces in the SD solver. For the applications presented in this paper, we transfer only the pressure contribution from the FD solution to the SD solver. Implementation of this iterative coupling is much more straightforward than direct coupling approaches. The separate treatment of the fluid and structural solvers allows us to use the two as subroutines in an FSI code. These reasons, along with the drawbacks of direct coupling approaches, have led most researchers in this field to focus on iterative coupling approaches.[3,4,25–27]

FSI information can be passed between the FD and SD solvers using compatible or incompatible meshes. Compatible meshes refer to the cases where the fluid-structure interface is represented by a nodally equivalent FD surface mesh and SD canopy mesh. Transfer of FSI information in this case is straightforward as a result of the one-to-one mapping between the interface nodes. Incompatible meshes refer to cases where the interface is represented by a FD surface mesh and a SD canopy mesh that are different. This approach has the benefit of allowing for individual FD and SD meshes to be designed to take advantage of the strengths of each solver. However, incompatible meshes require a more complicated projection scheme for transfer of information across the fluid-structure interface, such as a least-squares projection.[4,20] The least-squares projection, for transfer of FSI information between incompatible meshes, can be written as

$$\int_{\Gamma_{\mathrm{INT}}} \delta\boldsymbol{d}\cdot(\boldsymbol{d}^f - \boldsymbol{d}^s)\,\mathrm{d}\Gamma \tag{4}$$

where Γ_{INT} is the fluid-structure interface, $\boldsymbol{d}^f$ and $\boldsymbol{d}^s$ correspond to the shared variables between the fluid and the structure (i.e., displacements, displacement rates, and tractions), and $\delta\boldsymbol{d}$ is a test function associated with $\boldsymbol{d}^f$ or $\boldsymbol{d}^s$ (depending on which direction information is being transferred). For a parachute application, these two approaches are depicted in Fig. 1 with the fluid mesh (center) and compatible (left) and incompatible (right) SD meshes.

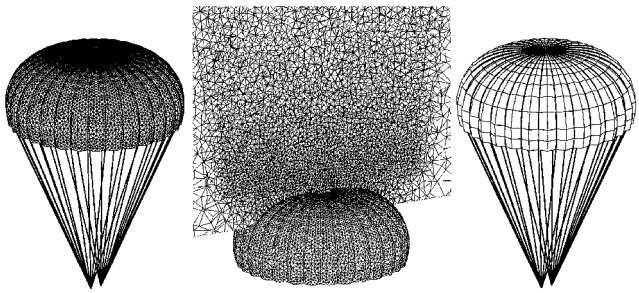

Fig. 1 Parachute meshes: compatible (left) vs incompatible (right).

Implementation

The FD and SD solvers are implemented using a message-passing paradigm and has been ported to a variety of architectures. Computations for the examples presented are carried out on a CRAY T3E-1200. The interested reader is directed to Kalro and Tezduyar[4] for further details of the parallel implementation.

Numerical Examples: Three-Dimensional FSI for a T-10 Parachute System

The Army's T-10 personnel parachute system is a "flat extended skirt canopy" composed of a 35-ft (10.67 m) diam D_c canopy and 30 suspension lines each 29.4 ft (8.96 m) long. The canopy is called a flat extended skirt canopy because in its constructed (or nonstressed) configuration it is composed of a main circular section with a circular vent at the apex and an inverted flat ring section, which lies under the main section and is connected to the main section at the outer radius. The lines connect to two confluence points (which approximate the connection points for a personnel harness assembly). The suspension lines continue as 30 gore-to-gore reinforcements through the parachute canopy and meet at the apex. For the T-10 the vent diameter is $0.1D_c$, and the width of the skirt is also $0.1D_c$.

In the following sections we describe the three-dimensional FSI strategy for numerical examples involving the T-10 parachute system. First, we will compare the numerical results corresponding to compatible and incompatible meshes. Second, we will demonstrate the simulation technique for a T-10 parachute/payload system during terminal descent. Finally, we will demonstrate the capability to perform "line pulls" during an FSI simulation.

Compatible vs Incompatible Meshes

SD Problem Setup

The simulations involve two SD models for the T-10. The first SD mesh (compatible case) consists of 9,183 nodes; 17,490 three-noded membrane elements for the canopy surface; and 1,920 two-noded cable elements for the suspension lines and canopy reinforcements. This SD mesh results in 27,543 equations.

The second SD mesh consists of 3,573 nodes; 780 nine-noded (i.e., biquadratic) membrane elements for the canopy surface; and 1,170 two-noded cable elements for the suspension lines and canopy reinforcements. This SD mesh results in 10,713 equations. The parachute system is represented by linearly elastic materials, with thickness and material properties representative of a T-10. Figure 2 shows "blown-out" views for the compatible and incompatible SD meshes for the main canopy reinforcements (cables), the main canopy (membranes), the extended skirt (membranes), and the extended skirt reinforcements and suspension lines (cables).

The unstructured mesh is allowed to inflate when the canopy is subjected to a prescribed differential pressure of 0.5 lb/ft^2 (23.94 Pa). For this stand-alone structural simulation every node in the SD mesh is unconstrained, with the exception of the two confluence point nodes, which are pinned. The fully inflated static configuration for the T-10 model obtained under the prescribed pressure loading is shown in Fig. 3. Maximum principal stresses for the parachute canopy (membrane) are superimposed on the surface, with low stresses along the canopy radial reinforcements and high stresses in the canopy midgore regions.

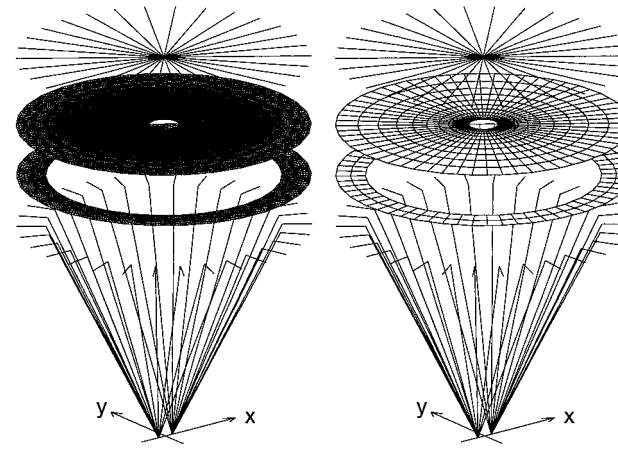

Fig. 2 Compatible and incompatible T-10 SD meshes.

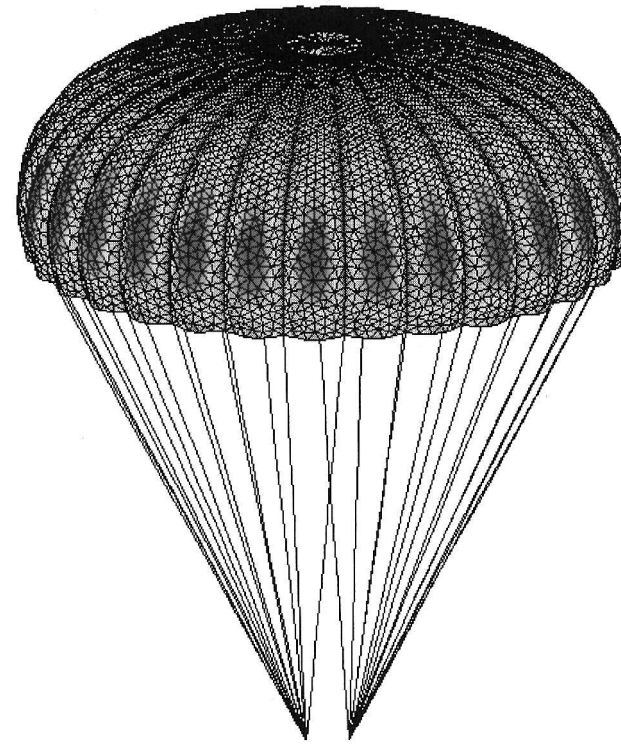

Fig. 3 Inflated T-10: SD geometry and stresses.

FD Problem Setup

A three-dimensional mesh with tetrahedral elements was generated for the FD solution using as the surface mesh the three-noded membrane mesh for the T-10 canopy in its inflated configuration. Canopy surface nodes were multiply defined, with one node for both the upper and lower surfaces. The mesh consists of 133,097 nodes and 783,910 tetrahedral elements. The flow simulations were carried out at a Reynold's number of 5×10^6 [which approximates the terminal descent velocity of 22.0 ft/s (6.7 m/s)]. Here, the Reynold's number is defined based on the constructed diameter of the canopy D_c. For this case the boundary conditions are defined as follows:

1) The *parachute canopy surface* is treated as a zero-porosity material and is assigned no-slip conditions.

2) The *inflow boundary below the parachute* is assigned a prescribed velocity condition of 22.0 ft/s (6.7 m/s).

3) The *side boundaries* are assigned free-slip conditions.

4) The *outflow boundary above the parachute* is assigned traction-free conditions.

Initial unsteady flow solutions were obtained for the fixed canopy configuration using a stabilized semidiscrete formulation.[22] The semidiscrete formulation, which is less cost intensive than the

DSD/SST formulation, is adequate for the stand-alone simulations because there is no time dependence in the spatial domain (i.e., no deformations of the canopy). Figure 4 shows a "snapshot" in time of the computed velocities and pressures for the flow about the T-10 canopy. After this flow is developed, several time steps were computed, still with the fixed canopy but by using the DSD/SST procedure, to obtain the starting FD conditions for the FSI simulation. For the DSD/SST procedure the FD system results in 958,686 equations. The computed drag coefficient for the stand-alone FD simulation, based on the total constructed area of the canopy, was approximately 0.72. This is without accounting for the suspension line or payload drag effects. The stand-alone simulation neglects FSI effects and thus is for a different canopy geometry than the expected FSI geometry. With the stated approximations in the stand-alone simulation, the computed drag compares quite acceptibly with the experimental values for the T-10 parachute system which range from 0.78 to 0.87

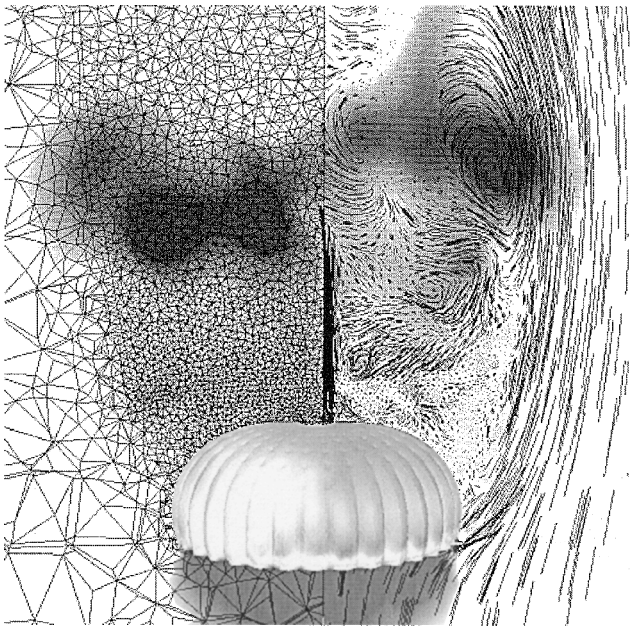

Fig. 4 Inflated T-10: Initial FD mesh and flowfield.

(Ref. 28) and include the payload drag, suspension line drag, and FSI effects.

FSI Simulation

FSI simulations were conducted for both the compatible and incompatible SD meshes. The FSI simulations were initiated using the fully inflated static configuration for the compatible mesh as the initial condition for the SD model and the fully developed flowfield about the fixed configuration as the initial condition for the flowfield. All SD nodes were prescribed to have no initial velocities or accelerations. The two payload nodes in the SD model were fully constrained. To begin the two FSI simulations with the same initial conditions, static equilibrium displacements from the compatible SD mesh were projected onto the incompatible SD mesh with a least-squares method.

Coupled simulations were carried out with a nondimensional time-step size of 0.005, which equates to a dimensional time step of 0.0032 s. The aerodynamic drag force acting on the canopy was calculated at each time step. Figure 5 shows the time histories for the nondimensional drag force. Good comparison is seen between the compatible and incompatible mesh simulations, with the incompatible mesh capturing higher-order modes of oscillation because of the higher-order biquadratic elements in the SD model. These oscillations are caused part by the snap through of individual gores as the parachute settles during the initial stages of the FSI simulation. Here, snap through refers to a local change in concavity of the canopy surface, which is resisted by compressive forces. For the problem presented there is no membrane wrinkling model implemented, and the triangular elements are unable to snap through for the given mesh resolution, whereas the higher-order membranes can experience the snap through. Realistic wrinkling models are being developed,[29] which effectively eliminate structural compressive stresses.

Freefalling T-10 Parachute System

SD Problem Setup

For this example, we modify the T-10 SD model to include a payload and a set of four risers connecting the payload to the suspension lines. We use the incompatible mesh from the preceding example as the base mesh for the parachute system. Each riser is represented by five two-noded cable elements. The front two risers each attach to seven suspension lines, and the back risers each

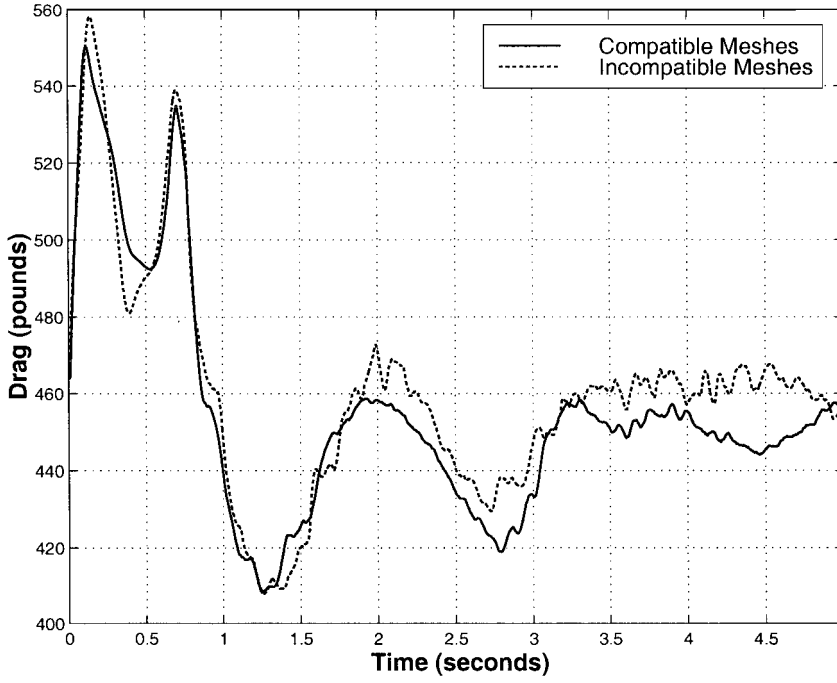

Fig. 5 Drag histories for both the compatible and incompatible simulations.

Table 1a T-10 parachute system: material properties

	Cables			Trusses
Material group	Suspension lines	Radial reinforcements	Risers	Payload
Elements	300	870	20	6
Area, ft^2	0.0001	0.0001	0.0001	0.0001
Density, $slugs/ft^3$	6.0	6.0	2.0	6.0
Young's modulus, lb/ft^2	4.32×10^6	4.32×10^6	2.16×10^7	4.65×10^9

Table 1b T-10 parachute system: material properties

	Membranes	Concentrated masses
Material group	Canopy	Payload masses
Elements	780	4
Thickness, ft	0.0001	——
Density (mass) $Slugs/ft^3$ (slugs)	6.0	(1.94)
Young's modulus, lb/ft^2	2.0×10^5	——
Poisson ratio	0.3	——

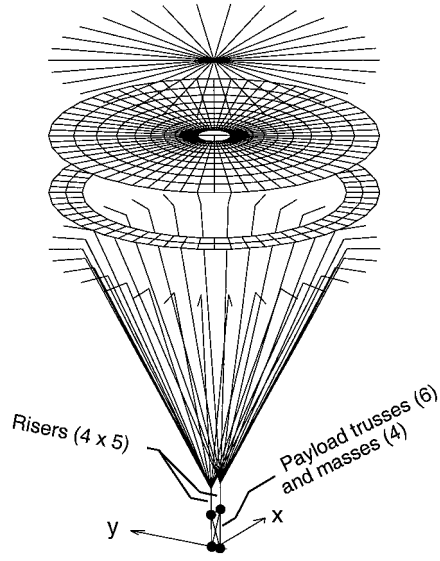

Fig. 6 SD mesh for T-10 with risers and payload.

attach to eight suspension lines. Additionally, each front and back riser attaches to the payload. The payload is represented by a stiff tetrahedral truss system and four concentrated mass elements. The six two-noded truss elements give the payload structure rigidity, and the four concentrated masses approximate the mass of a typical paratrooper. This payload modeling technique has been demonstrated for three-dimensional stand-alone SD simulations.[23] The blown-out depiction of the SD mesh for the T-10 parachute system with risers and payload is shown in Fig. 6.

The SD model is broken into six distinct material groups: one membrane group, three cable groups, a truss group, and a concentrated mass group. The membrane group defines the parachute canopy. We have distinct cable groups for the suspension lines, the canopy radial reinforcements, and the risers. The truss and concentrated mass groups define the payload. The definitions for the different material groups are given in Tables 1a and 1b.

A stand-alone damped dynamic simulation was conducted for the T-10 parachute model to inflate the canopy under a prescribed differential pressure of 0.5 lb/ft^2 (23.94 Pa). For the stand-alone simulation the four payload node points were fixed in space. This equilibrium solution is used as the initial condition for the SD solver in the subsequent FSI simulation.

FD Problem Setup

The canopy surface unstructured mesh with triangular elements was generated by first generating a mesh for the flat canopy and then projecting the displacements from the SD equilibrium solution onto the flat mesh. This mesh is used to represent the T-10 canopy as an interior surface in the FD mesh. A three-dimensional mesh with tetrahedral elements was generated, with 149,253 nodes and 888,344 elements. The unsteady flow solutions to be used as starting conditions for the FSI simulation were obtained for the fixed canopy configuration at Reynolds number of 5×10^6 using a semidiscrete formulation. This solution was used as the initial condition for the FSI simulation, which were carried out using the DSD/SST procedure.

FSI Simulation

For the preceding example we simulated the FSI behavior for the flow about a T-10 parachute, where the payload was fixed in

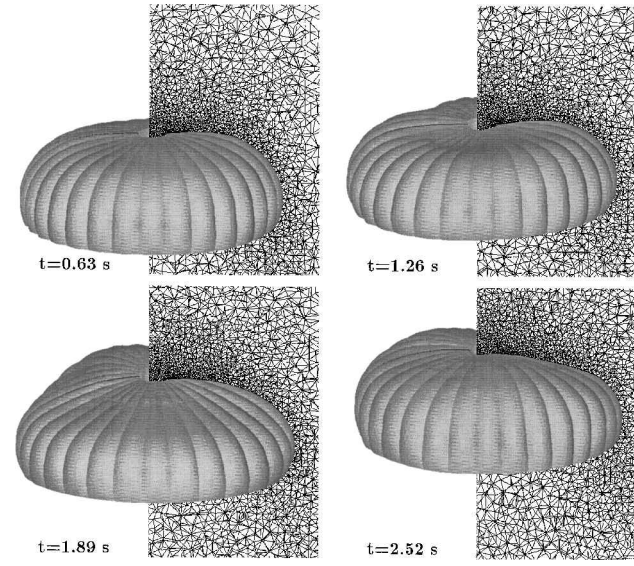

Fig. 7 FD mesh during FSI simulation.

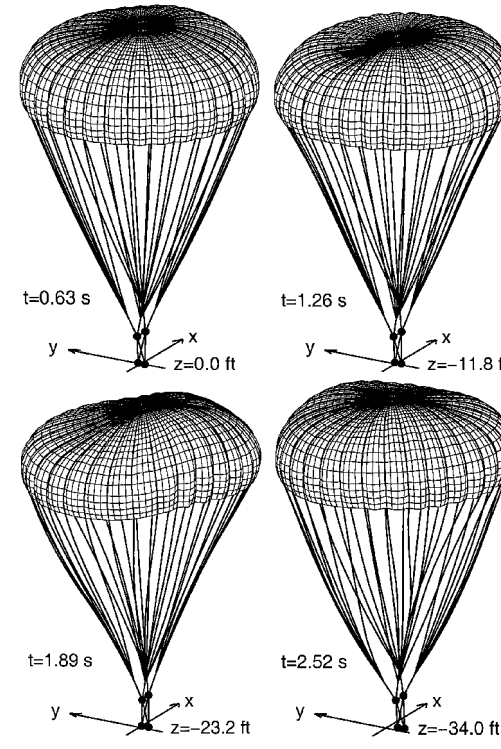

Fig. 8 SD mesh during FSI simulation.

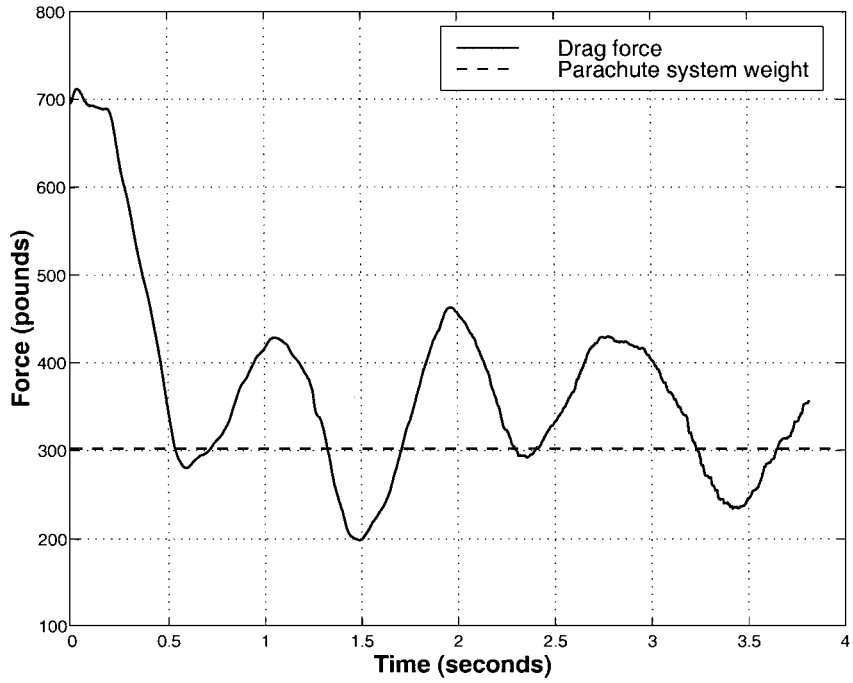

Fig. 9 Drag force.

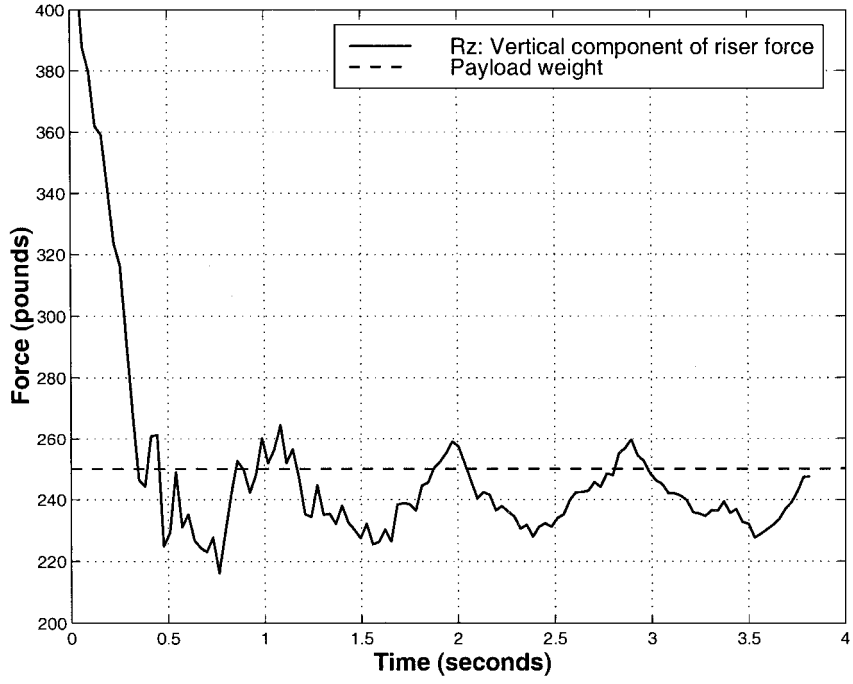

Fig. 10 Net vertical riser force.

space. For this case, where the parachute is allowed to freefall, the parachute structure will fall (or rise) globally at some velocity relative to the inflow velocity. Thus, the predicted terminal descent for the parachute system will be the terminal SD velocity plus the inflow velocity. This combined Lagrangian–Eulerian description for the problem was selected to simplify the setup for the initial conditions of the FSI problem.

To handle the freefalling parachute, we implement our automatic mesh-moving scheme as follows:

1) The *parachute canopy surface* is assigned a prescribed displacement condition, with the prescribed displacements coming from the SD solution.

2) The *outer mesh boundaries* are assigned prescribed displacement conditions, with displacements equal to the average SD canopy displacements (i.e., the FD mesh moves globally with the parachute canopy).

3) Interior mesh points are updated based on the pseudosolid automatic mesh-moving strategy.

The FSI simulation is initiated using the equilibrium solution for the SD solver and the initial condition generated for the FD solver. At the onset of the simulation, the payload nodes in the SD model are no longer fixed in space, and the parachute SD model is fully unconstrained. Motion of the structure is driven by the external forces (i.e., gravity, line drag, payload drag), the internal forces, and the FD-induced pressures on the canopy. Likewise, the FD solution is driven by the prescribed inflow condition and the structural displacements and displacement rates on the canopy surface. The initial condition for the FSI simulation is not in a coupled fluid and

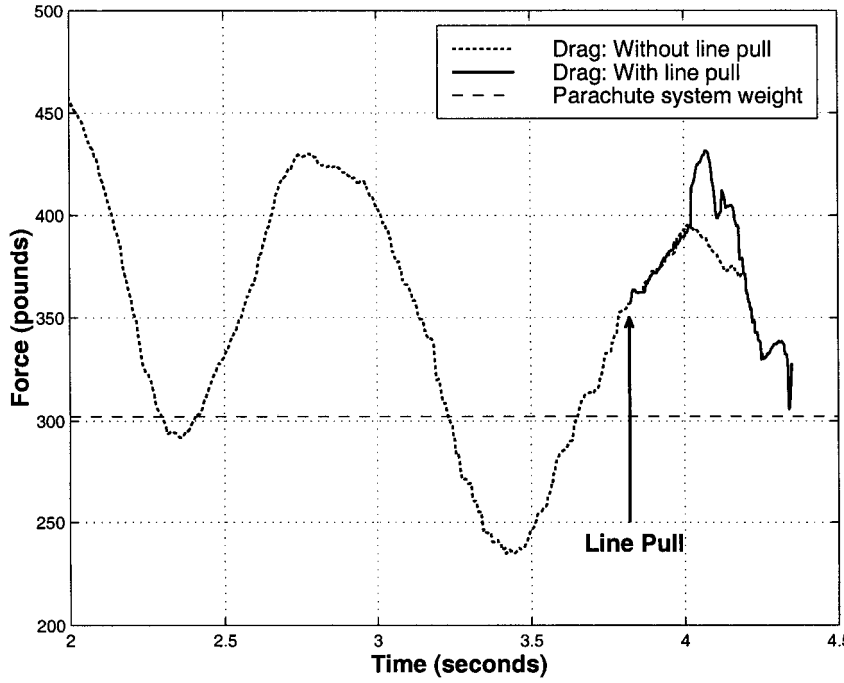

Fig. 11 Soft-landing drag force.

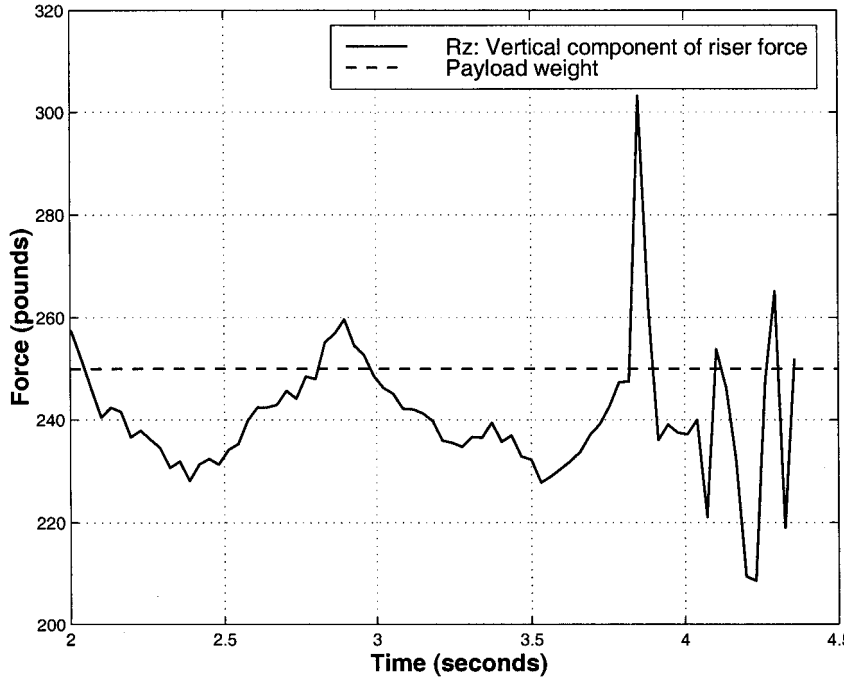

Fig. 12 Soft-landing net vertical riser force.

structural equilibrium state. Therefore, the parachute structure experiences a large amount of settling during the initial stages of the FSI simulation. Figures 7 and 8 show the behavior of the FD and SD meshes at four instants during the FSI simulation, with 0.63 s of real time between each instant. In Fig. 7 we show, for the FD mesh, the deforming canopy surface and a section in a fixed cutting plane. The combined Lagrangian–Eulerian reference frame for the FSI simulation is evident by the fact that the canopy rises relative to the fixed cutting plane in this sequence of pictures. In Fig. 8 we show the deforming T-10 structural model for the same four instants. Severe deformations in the parachute canopy and suspension lines are clearly seen. Also evident are motions of the payload in lateral directions. In addition, the figures show the vertical position of the payload.

Figure 9 shows the time history of the aerodynamic drag force acting on the parachute canopy. The dashed line corresponds to the total gravitational force acting on the parachute system (i.e., canopy, suspension lines, risers, and payload weights). As expected, the drag force oscillates about the weight of the parachute system. Figure 10 shows the time history of the net vertical tension forces that the risers exert on the payload. The force contributions caused by the payload drag approximations are very small (i.e., less than one pound), and, therefore, the net vertical riser force effectively balances the 250-lb (1112 N) payload, as seen in Fig. 10.

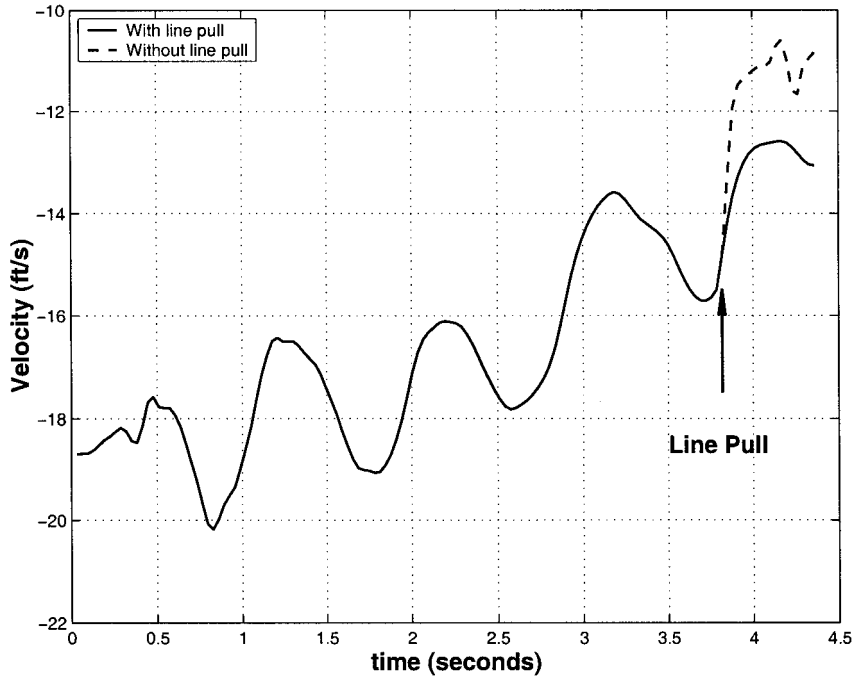

Fig. 13 Soft-landing payload velocity.

T-10 Control Line Pull

Being able to represent time-variant cable lengths during an FSI simulation is necessary to represent several important parachute operations. These operations include control line "pulls" and "releases" in parachute maneuvering, riser pulls during soft landing, control line pulls for maneuvers and flared landings of ram-air parachutes, and dis-reefing. Various control line operations have been reported for SD stand-alone simulations.[23]

A "soft landing" was simulated at the end of the T-10 FSI simulation presented in the preceding section. This was accomplished by smoothly decreasing in time the natural lengths of the cable elements defining the four risers. During the simulation, over a 0.5-s interval, the risers were each decreased from 3.0 ft (0.91 m) to approximately 2.0 ft (0.61 m). Figure 11 shows the computed drag throughout the simulation with the line pull starting between 3.5 and 4.5 s. As expected, higher drag is predicted for the line-pull case. However, there is a delayed response in the aerodynamic drag on the canopy caused by the line pull, which results from the elasticity in the the parachute structure and the structural response response to the line pull.

Figure 12 shows the net vertical force in the four risers prior to and throughout the soft landing simulation. Here, the response to the line pull is immediate, as expected. Figure 13 shows the vertical payload velocity throughout the simulation with and without the line pull. The reduction in the vertical payload velocity caused by the soft landing is evident in this figure. Additional simulations can be carried out to provide further information on possible soft landings and for line pulls of different magnitudes and durations.

Conclusions

Parachute operations involve highly deformable structures interacting with complex flowfields. Being able to predict parachute behavior requires modeling of highly nonlinear fluid-structure interactions. The simulation capability for this complex application has been attainable only recently, with development of advanced computational methods and availability of powerful computers. In this paper we presented a method for carrying out simulations for parachute fluid-structure interactions that can be applied to a broad range of parachute systems. The method includes the fluid and structural dynamics models and the coupling strategy developed for this purpose. Several test applications for a T-10 parachute were also presented to demonstrate this computational capability.

Acknowledgments

This work was sponsored in part by U.S. Air Force of Scientific Research (Contract F49620-98-1-0214), by NASA-JSC (Grant NAG9-1059) and by the Army High Performance Computing Research Center under the auspices of the U.S. Department of the Army, Army Research Laboratory cooperative agreement DAAH04-95-2-0003 and Contract DAAH04-95-C-0008. The content does not necessarily reflect the position or the policy of the government, and no official endorsement should be inferred.

References

[1] Peterson, C. W., Strickland, J. H., and Higuchi, H., "The Fluid Dynamics of Parachute Inflation," *Annual Review of Fluid Mechanics*, Vol. 28, 1996, pp. 361–387.

[2] Benney, R. J., and Stein, K. R., "A Computational Fluid Structure Interaction Model for Parachute Inflation," *Journal of Aircraft*, Vol. 33, No. 4, 1996, pp. 730–736.

[3] Stein, K., Benney, R., Kalro, V., Tezduyar, T., Leonard, J., and Accorsi, M., "Parachute Fluid-Structure Interactions: 3-D Computation," *Computer Methods in Applied Mechanics and Engineering*, Vol. 190, 2000, pp. 373–386.

[4] Kalro, V., and Tezduyar, T., "A Parallel Finite Element Methodology for 3D Computation of Fluid-Structure Interactions in Airdrop Systems," *Proceedings of the 4th Japan-US Symposium on Finite Element Methods in Large-Scale Computational Fluid Dynamics*, Funabashi, Japan, 1998.

[5] Ibos, C., Lacroix, C., Goy, A., and Bordenave, P., "Fluid-Structure Simulation of 3D Ram Air Parachute with Sinpa Software," *Proceedings of the Confederation of European Aerospace Societies/AIAA 15th Aerodynamic Decelerator Systems Technology Conference*, AIAA 99-1714, AIAA, Reston, VA, 1999, pp. 88–98.

[6] Mosseev, Y., "The Decelerator Pitch-Dependent Performances Prediction Based on 3D Aeroelastic Analysis," *Proceedings of the Confederation of European Aerospace Societies/AIAA 15th Aerodynamic Decelerator Systems Technology Conference*, AIAA 99-1717, AIAA, Reston, VA, 1999, pp. 129–137.

[7] Tezduyar, T. E., Behr, M., and Liou, J., "A New Strategy for Finite Element Computations Involving Moving Boundaries and Interfaces—the Deforming-Spatial-Domain/Space-Time Procedure: I. The Concept and the Preliminary Tests," *Computer Methods in Applied Mechanics and Engineering*, Vol. 94, 1992, pp. 339–351.

[8] Tezduyar, T. E., Behr, M., Mittal, S., and Liou, J., "A New Strategy for Finite Element Computations Involving Moving Boundaries and Interfaces—the Deforming-Spatial-Domain/Space-Time Procedure: II. Computation of Free-Surface Flows, Two-Liquid Flows, and Flows with Drifting Cylinders," *Computer Methods in Applied Mechanics and Engineering*, Vol. 94, 1992, pp. 353–371.

[9]Smagorinsky, J., "General Circulation Experiments with the Primitive Equations," *Monthly Weather Review*, Vol. 91, 1963, pp. 99–165.

[10]Benney, R. J., and Leonard, J. W., "A 3-D Finite Element Structural Parachute Model," *Proceedings of the 13th AIAA Aerodynamic Decelerator Systems Technology Conference*, AIAA 95-1563, 1995, pp. 165–175.

[11]Benney, R. J., Stein, K. R., Leonard, J. W., and Accorsi, M. L., "Current 3-D Structural Dynamic Finite Element Modeling Capabilities," *Proceedings of the 14th AIAA Aerodynamic Decelerator Systems Technology Conference*, AIAA 97-1506, AIAA, Reston, VA, 1997, pp. 285–303.

[12]Kalro, V., Aliabadi, S., Garrard, W., Tezduyar, T., Mittal, S., and Stein, K., "Parallel Finite Element Simulation of Large Ram-Air Parachutes," *International Journal for Numerical Methods in Fluids*, Vol. 24, 1997, pp. 1353–1369.

[13]Mittal, S., and Tezduyar, T. E., "A Finite Element Study of Incompressible Flows Past Oscillating Cylinders and Airfoils," *International Journal for Numerical Methods in Fluids*, Vol. 15, 1992, pp. 1073–1118.

[14]Mittal, S., and Tezduyar, T. E., "Massively Parallel Finite Element Computation of Incompressible Flows Involving Fluid-Body Interactions," *Computer Methods in Applied Mechanics and Engineering*, Vol. 112, 1994, pp. 253–282.

[15]Mittal, S., and Tezduyar, T. E., "Parallel Finite Element Simulation of 3D Incompressible Flows—Fluid-Structure Interactions," *International Journal for Numerical Methods in Fluids*, Vol. 21, 1995, pp. 933–953.

[16]Wren, G., Ray, S., Aliabadi, S., and Tezduyar, T., "Simulation of Flow Problems with Moving Mechanical Components, Fluid-Structure Interactions and Two-Fluid Interfaces," *International Journal for Numerical Methods in Fluids*, Vol. 24, 1997, pp. 1433–1448.

[17]Stein, K. R., Benney, R. J., Kalro, V., Johnson, A. A., and Tezduyar, T. E., "Parallel Computation of Parachute Fluid-Structure Interactions," *Proceedings of the 14th AIAA Aerodynamic Decelerator Systems Technology Conference*, AIAA 97-1505, AIAA, Reston, VA, 1997, pp. 277–284.

[18]Stein, K., Benney, R., Kalro, V., Tezduyar, T., Bretl, T., and Potvin, J., "Fluid-Structure Interaction Simulations of a Cross Parachute: Comparisons of Numerical Predictions with Wind Tunnel Data," *Proceedings of the Confederation of European Aerospace Societies/AIAA 15th Aerodynamic Decelerator Systems Technology Conference*, AIAA 99-1725, AIAA, Reston, VA, 1999, pp. 172–181.

[19]Brocato, B., Esteve, L., Garcia, D., Manglano, C., Peek, G., Potvin, J., Benney, R., Stein, K., Alamat, R., and Little, J., "Experimental Study of Fluid-Structure Interactions on a Cross Parachute: Comparison of Wind Tunnel Data and Drop Data with CFD Predictions," *Proceedings of the Confederation of European Aerospace Societies/AIAA 15th Aerodynamic Decelerator Systems Technology Conference*, AIAA 99-1737, AIAA, Reston, VA, 1999, pp. 269–278.

[20]Maman, N., and Farhat, C., "Matching Fluid and Structure Meshes for Aeroelastic Computations: A Parallel Approach," *Computers and Structures*, Vol. 54, 1995, pp. 779–785.

[21]Brooks, A. N., and Hughes, T. J. R., "Streamline Upwind/Petrov–Galerkin Formulations for Convection Dominated Flows with Particular Emphasis on the Incompressible Navier–Stokes Equations," *Computer Methods in Applied Mechanics and Engineering*, Vol. 32, 1982, pp. 199–259.

[22]Tezduyar, T. E., "Stabilized Finite Element Formulations for Incompressible Flow Computations," *Advances in Applied Mechanics*, Vol. 28, 1991, pp. 1–44.

[23]Benney, R., Stein, K., Zhang, W., Accorsi, M., and Leonard, J., "Controllable Airdrop Simulations Utilizing a 3-D Structural Dynamics Model," *Proceedings of the Confederation of European Aerospace Societies/AIAA 15th Aerodynamic Decelerator Systems Technology Conference*, AIAA 99-1727, AIAA, Reston, VA, 1999, pp. 182–192.

[24]Tezduyar, T. E., Behr, M., Mittal, S., and Johnson, A. A., "Computation of Unsteady Incompressible Flows with the Stabilized Finite Element Methods-Space-Time Formulations, Iterative Strategies and Massively Parallel Implementations," *New Methods in Transient Analysis*, edited by P. Smolinski, W. K. Liu, G. Hulbert, and K. Tamma, AMD-Vol. 143, American Society of Mechanical Engineers, New York, 1992, pp. 7–24.

[25]Farhat, C., Lesoinne, M., and Maman, N., "Mixed Explicit/Implicit Time Integration of Coupled Aeroelastic Problems: Three-Field Formulation, Geometric Conservation, and Distributed Solution," *International Journal for Numerical Methods in Fluids*, Vol. 21, 1995, pp. 807–835.

[26]Farhat, C., and Lesoinne, M., "Higher-Order Staggered and Subiteration Free Algorithms for Coupled Dynamic Aeroelasticity Problems," *Proceedings of the 36th AIAA Aerospace Sciences Meeting*, AIAA, Reston, VA, 1998.

[27]Löhner, R., Yang, C., Cebral, J., Baum, J. D., Luo, H., Pelessone, D., and Charman, C., "Fluid-Structure Interaction Using a Loose Coupling Algorithm and Adaptive Unstructured Grids," *Proceedings of the 36th AIAA Aerospace Sciences Meeting*, AIAA, Washington, DC, 1995.

[28]Ewing, E. G., Bixby, H. W., and Knacke, T. W., "Recovery Systems Design Guide," U.S. Air Force Rept. AFFDL-TR-78-151, 1978.

[29]Accorsi, M., Lu, K., Leonard, J., Benney, R., and Stein, K., "Issues in Parachute Structural Modeling: Damping and Wrinkling," *Proceedings of the Confederation of European Aerospace Societies/AIAA 15th Aerodynamic Decelerator Systems Technology Conference*, AIAA 99-1729, AIAA, Reston, VA, 1999, pp. 193–204.